

First-order phase transitions in two-dimensional off-lattice liquid crystals

H. H. Wensink and R. L. C. Vink

*Institut für Theoretische Physik II: Weiche Materie,
Heinrich-Heine-Universität Düsseldorf, Universitätsstraße 1, 40225 Düsseldorf, Germany*

(Dated: November 4, 2018)

We consider an *off-lattice* liquid crystal pair potential in strictly two dimensions. The potential is purely repulsive and short-ranged. Nevertheless, by means of a single parameter in the potential, the system is shown to undergo a first-order phase transition. The transition is studied using mean-field density functional theory, and shown to be of the isotropic-to-nematic kind. In addition, the theory predicts a large density gap between the two coexisting phases. The first-order nature of the transition is confirmed using computer simulation and finite-size scaling. Also presented is an analysis of the interface between the coexisting domains, including estimates of the line tension, as well as an investigation of anchoring effects.

PACS numbers: 64.70.Md, 02.70.-c, 61.30.Cz, 61.30.Hn

I. INTRODUCTION

The phase behavior of liquid crystals in two dimensions continues to be an interesting topic. On the one hand, at least for *lattice* liquid crystals, there is a clear resemblance to the planar spin or XY-model [1]. In fact, the Lebwohl-Lasher (LL) model [2], which is one of the standard liquid crystal models, maps exactly onto the XY-model in two dimensions. The XY-model does not support long-range order [3] and, consequently, long-range nematic order is believed to be absent in many two-dimensional (2D) liquid crystals as well [4, 5, 6] (an exception being Ref. 7). In addition, the XY-model features a Kosterlitz-Thouless (KT) transition [8, 9]. Consequently, phase transitions in two-dimensional liquid crystals are often interpreted in terms of the KT scenario [4, 5, 6, 10, 11]. In particular, the KT transition is a *continuous* transition, as opposed to first-order. As a result, the possibility of a first-order transition occurring in a two-dimensional liquid crystal, has received relatively little attention.

Interestingly, computer simulations of appropriately *generalized* XY-models have shown that the possibility of also a first-order transition occurring in these systems should be taken seriously [12, 13, 14]. More recently, these findings were put on firm mathematical ground by van Enter and Shlosman [15, 16, 17]. In particular, it was demonstrated that Hamiltonians of the form

$$\mathcal{H}_{\text{gXY}} = - \sum_{\langle i,j \rangle} \left(\frac{1 + \hat{\omega}_i \cdot \hat{\omega}_j}{2} \right)^p, \quad (1)$$

undergo first-order phase transitions when p is large [17]. In Eq. (1), the sum is over nearest neighbors on a square lattice, and $\hat{\omega}_i$ are two-dimensional unit vectors. The usual XY-model (up to a trivial constant and multiplicative factor) is recovered for $p = 1$; the generalization is to also consider $p \gg 1$. In computer simulations, the first-order transition was already observed at $p = 50$ [12]. Of course, for small p , the KT-scenario is ultimately recovered again, for which the transition is continuous.

The results obtained for generalized XY-models have similar consequences for two-dimensional liquid crystals. This was recently demonstrated in Ref. 18 using a generalized version of the LL-model

$$\mathcal{H}_{\text{gLL}} = - \sum_{\langle i,j \rangle} |\hat{\omega}_i \cdot \hat{\omega}_j|^p, \quad (2)$$

the essential difference with Eq. (1) being inversion symmetry under $\hat{\omega}_i \leftrightarrow -\hat{\omega}_i$ of the particle orientations. In particular, it was shown that Eq. (2) undergoes a first-order temperature-driven transition, from an isotropic to a quasi-nematic phase, provided p is sufficiently large. Again, the threshold value is at $p \approx 50$ [18]. In the isotropic phase, the orientational correlations decay exponentially; in the quasi-nematic phase, they decay algebraically. Both phases thus lack long-range order in the thermodynamic limit, in agreement with the Mermin-Wagner theorem [3]. Consequently, the nematic order parameter cannot be used to describe the first-order transition in Eq. (2). Instead, a valid order parameter is the energy density, which shows a “jump” at the transition temperature. By keeping the energy density fixed at some value in the coexistence region, phase coexistence between isotropic and quasi-nematic domains can be realized [18].

The aim of this paper is to investigate how robust these findings are when also *off-lattice* liquid crystals in two dimensions are considered. To this end, we formulate an *off-lattice* model of a liquid crystal, which is somewhat inspired by the lattice Hamiltonian of Eq. (2). The model will be presented in Section II. Next, the phase behavior of this model is studied, using theory and simulation. Indeed, both the theory and the simulation find strong evidence for the existence of a first-order transition, including a pronounced coexistence region. The coexistence region will be analyzed in some detail, including estimates of the line tension between the coexisting domains. An important improvement over the lattice model of Eq. (2) is that the transition in the *off-lattice* model is characterized by a “jump” in the particle density. In other words, phase coexistence can now be studied by

keeping the overall particle density fixed at some appropriate value, rather than the energy density. This finding is relevant for possible experiments, where the condition of fixed density is rather easy to implement (in contrast, keeping the overall energy fixed in an experiment would be much more difficult). At the same time, we find that the analogue of the p -exponent in Eq. (2) must be quite large, before the first-order transition begins to show-up. Whether such “sharp” interactions can be realized experimentally is not yet clear, but some suggestions are made toward the end of this paper.

II. OFF-LATTICE LIQUID CRYSTAL IN TWO DIMENSIONS

In this paper, we consider an ensemble of particles, whose positions and orientations are confined to a two-dimensional plane. The particles interact with each other via a pair potential v_{ij} of the form

$$v_{ij} = \epsilon \sigma_{ij} (1 - |\hat{\omega}_i \cdot \hat{\omega}_j|^p) u(r), \quad (3)$$

$$\sigma_{ij} = 1 + \nu [(\hat{\omega}_i \cdot \mathbf{r}_{ij}/r)^2 + (\hat{\omega}_j \cdot \mathbf{r}_{ij}/r)^2], \quad (4)$$

with $\mathbf{r}_{ij} = \mathbf{r}_j - \mathbf{r}_i$, $r = |\mathbf{r}_{ij}|$, $-1/2 < \nu < 1/2$, and coupling parameter $\epsilon > 0$. In what follows, factors of $k_B T$ are absorbed into the parameter ϵ , with T the temperature, and k_B the Boltzmann constant. The quantity $\hat{\omega}_i$ is a two-dimensional unit vector denoting the orientation of the i -th particle; \mathbf{r}_i is a two-dimensional vector denoting the coordinate of the center of mass of the i -th particle. The radial function $u(r)$ in Eq. (3) is assumed to be strictly positive and short-ranged. Here, we take a simple step function

$$u(r) = \begin{cases} 1 & r < a, \\ 0 & \text{otherwise,} \end{cases} \quad (5)$$

with a the particle diameter which will henceforth serve as our unit of length.

As for the lattice Hamiltonian of Eq. (2), the potential is constructed such that inversion symmetry is maintained. Note also that v_{ij} is purely repulsive. Nevertheless, we expect a first-order phase transition to take place, either at low temperature, or at high density, provided p is large. The purpose of the parameter ν is to introduce a coupling between the orientational and translational degrees of freedom. By setting $\nu = 0$, no such coupling occurs, and the potential becomes separable. For this special case, Straley has rigorously proved the absence of long-range nematic order [19]. As far as we know, the absence or presence of long-range order for the case $\nu \neq 0$ is still an open question.

III. DENSITY FUNCTIONAL THEORY

Within density functional theory (DFT) the thermodynamics and structure of a fluid is described by a func-

tional $\Omega[\rho]$ of the one-particle distribution $\rho(\mathbf{r}, \hat{\omega})$. The density functional is such that it is minimized for a given (μ, A, T) by the equilibrium one-particle distribution and the minimum value of the functional is the grand potential [20] (in the present study in two dimensions, A is the system area). Here we use a simple mean-field functional which, in the absence of an external potential, can be cast in the following form

$$\Omega[\rho] = \int d\mathbf{r} d\hat{\omega} \rho(\mathbf{r}, \hat{\omega}) (\ln[\mathcal{V}\rho(\mathbf{r}, \hat{\omega})] - 1 - \mu) \quad (6)$$

$$+ \frac{1}{2} \int d\mathbf{r} d\hat{\omega} \int d\mathbf{r}' d\hat{\omega}' v(\Delta\mathbf{r}; \hat{\omega}, \hat{\omega}') \rho(\mathbf{r}, \hat{\omega}) \rho(\mathbf{r}', \hat{\omega}'),$$

with Ω expressed in units $k_B T$, $\Delta\mathbf{r} = \mathbf{r}' - \mathbf{r}$, \mathcal{V} the 2D thermal volume of the particle and μ the chemical potential. The functional is known to give accurate results for dense fluids of soft spheres with bounded potentials [21, 22, 23]. Recently, it was shown that the approach also works well for fluids of soft anisometric particles [24]. The minimum condition on the functional, $\delta\Omega[\rho]/\delta\rho = 0$, leads to a nonlinear integral equation

$$\ln[\mathcal{V}\rho(\mathbf{r}, \hat{\omega})] + \int d\mathbf{r}' d\hat{\omega}' v(\Delta\mathbf{r}; \hat{\omega}, \hat{\omega}') \rho(\mathbf{r}', \hat{\omega}') = \mu, \quad (7)$$

to be solved for the equilibrium distribution $\rho(\mathbf{r}', \hat{\omega}')$ at a given μ .

A. Bulk phase diagram

Let us first focus on localizing the isotropic-to-nematic transition for bulk systems. As the average density in both states is spatially *uniform*, i.e. independent of \mathbf{r} , we may write $\rho(\mathbf{r}, \hat{\omega}) = \rho f(\hat{\omega})$, where ρ is the bulk density and f an orientational distribution, subject to the normalization condition $\int d\hat{\omega} f(\hat{\omega}) = 1$. In the isotropic (I) state, all orientations are equally probable and f_I is a constant while in the nematic (N) phase f_N is expected to be strongly peaked around the nematic director which we assume to be spatially uniform. This implies that long-range orientational order is always present in theory since fluctuations or local defects in the director field are not taken into account. Introducing the angle $\varphi \in [0, \pi]$ between the particle and the nematic director we may rewrite Eq. (7) into a self-consistency equation for $f(\varphi)$

$$f(\varphi) = Z^{-1} \exp \left[-\rho \int d\varphi' E(\varphi, \varphi') f(\varphi') \right], \quad (8)$$

where $Z = \int d\varphi \exp[\dots]$ to ensure normalization. Note that $f(\varphi) = f(\pi - \varphi)$ due to the inversion symmetry. The kernel $E(\varphi, \varphi')$ is given by the following spatial integration

$$E(\varphi, \varphi') = \int d\Delta\mathbf{r} v(\Delta\mathbf{r}; \hat{\omega}, \hat{\omega}'). \quad (9)$$

The spatial integration in Eq. (9) can then be carried out without difficulty to give

$$E(\varphi, \varphi') = \epsilon(1 + \nu)\pi a^2 (1 - |\cos(\varphi' - \varphi)|^p). \quad (10)$$

With this result it is expedient to rewrite Eq. (8) in the following way

$$f(\varphi) = Z^{-1} \exp \left[c \int d\varphi' |\cos(\varphi' - \varphi)|^p f(\varphi') \right], \quad (11)$$

where we have introduced the *effective* dimensionless density

$$c = \pi(1 + \nu)\rho a^2 \epsilon. \quad (12)$$

The combination $\rho\epsilon$ in Eq. (12) illustrates the fact that phase transitions in our model can be brought about by either increasing the density or lowering the temperature. It is clear that the isotropic distribution $f_I = 1/\pi$ is a trivial solution of Eq. (11) at all densities c . However at high densities non-trivial, i.e. nematic solutions are expected to branch off from the isotropic one. To locate the branching point (denoted by c^*) we will perform a simple stability analysis of Eq. (11), along the lines of Refs. 25, 26. Let us introduce the following expansions around the isotropic solution

$$\begin{aligned} f(\varphi) &= \frac{1}{\pi} [1 + \alpha a_1 \cos 2\varphi + \alpha^2 a_2 \cos 4\varphi + \dots], \\ c &= c_0 + \alpha c_1 + \alpha^2 c_2 + \dots, \end{aligned} \quad (13)$$

in terms of a single order parameter α . Likewise, we may expand the kernel as follows

$$|\cos(\varphi' - \varphi)|^p = \sum_{n \geq 0} k_{2n}(p) \cos(2n\varphi) \cos(2n\varphi'), \quad (14)$$

with coefficients

$$\begin{aligned} k_{2n}(p) &= \\ \frac{4}{\pi^2} \int d\varphi \int d\varphi' |\cos(\varphi' - \varphi)|^p \cos(2n\varphi) \cos(2n\varphi'). \end{aligned} \quad (15)$$

Inserting all expansions back into Eq. (11) and keeping all contributions up to $\mathcal{O}(\alpha)$ gives the branching or bifurcation point

$$c^* = c_0 = 2/k_2(p), \quad (16)$$

implying that stable nematic solutions are expected for $c > c^*$. We remark that for $p = 1$ the branching density $c^* = 3\pi/2$ is identical to that of the 2D Onsager theory for infinitely thin hard needles [19, 27].

To verify the thermodynamic stability of the nematic solutions close to the branching density we must analyze its free energy. The dimensionless Helmholtz free energy (ignoring all irrelevant constants) is given by

$$F[f]/N \sim \langle \ln[c\pi f(\varphi)] \rangle + \frac{c}{2} \langle \langle (1 - |\cos(\varphi' - \varphi)|^p) \rangle \rangle, \quad (17)$$

where $\langle \dots \rangle = \int d\varphi f(\varphi)$. The free energy difference $\Delta F = F_N - F_I$ between the nematic and isotropic states close to the branching point can be written in Landau form in terms of the nematic order parameter α

$$\Delta F/N = A\alpha^2 + B\alpha^3 + C\alpha^4. \quad (18)$$

The coefficients can be obtained from extending the bifurcation analysis to higher order in α [using the expansions Eq. (13) and Eq. (14)] and performing an order-by-order solution of Eq. (11) up to $\mathcal{O}(\alpha^3)$. The algebra is straightforward but tedious and we will only give the final outcome here. It turns out that $A, B = 0$ while

$$C = -\frac{k_2(p) - 2k_4(p)}{64[k_2(p) - k_4(p)]}. \quad (19)$$

The order of the transition depends on the sign of C . If it is negative, small nematic perturbations around the branching point immediately stabilize the system and the transition is continuous. If C is positive the incipient free energy difference goes up for small α which means that the actual phase transition must involve a density jump and is first-order. In the latter case the coexisting densities are indicated by binodal curves which can be computed in the usual way by requiring the pressure and chemical potential to be equal in the coexisting phases. The equilibrium $f(\varphi)$ for a given nematic density c is obtained numerically from the consistency equation Eq. (11) by dividing the interval $[0, \pi/2]$ into 100 equidistant grid points and employing the iteration scheme outlined in Ref. 28.

Fig. 1 shows that the isotropic-nematic transition is continuous for small p but becomes first-order for $p > 8$. The full phase diagram in Fig. 2 shows that the actual crossover from continuous to first-order (marked by the tri-critical point where all phase lines meet) is located at a somewhat lower value for p , namely $p = 4.7$. The discrepancy is expected since the bifurcation analysis usually provides an *upper* estimate for the critical points. We also remark that the non-monotonic behavior of the critical density at low p is consistent with the simulation results of the generalized LL-model reported in Ref. 18. The steep increase of the nematic order parameter in Fig. 3 suggests that a considerable degree of nematic order is expected in the coexisting nematic phase at large p .

1. Asymptotic results for large p

For very large p (say larger than 100) the solution of Eq. (11) on a grid becomes numerically awkward since $f(\varphi)$ gets extremely peaked at $\varphi = 0$ (and π). It is therefore tempting to formulate a simple variational theory that allows us to access the phase diagram at asymptotically large p . Indeed, for highly nematic states $f(\varphi)$ is well-described by a gaussian trial function with variational parameter $\beta \gg 1$ [29],

$$f(\varphi) \sim \left(\frac{2\beta}{\pi} \right)^{1/2} \exp \left[-\frac{1}{2} \beta \varphi^2 \right], \quad \text{for } 0 \leq \varphi \leq \frac{\pi}{2}, \quad (20)$$

and its mirrored version $f(\pi - \varphi)$ for the interval $\pi/2 \leq \varphi \leq \pi$. Inserting the gaussian into Eq. (17) and integrating yields the following asymptotic result for the ideal free energy (first term)

$$\begin{aligned} \langle \ln[c\pi f(\varphi)] \rangle &\sim \ln c + \frac{1}{2} \ln 2\pi\beta - \frac{1}{2}, & \text{(N)} \\ &= \ln c, & \text{(I)} \end{aligned} \quad (21)$$

valid for large β . Using the approximation

$$|\cos x|^p \approx \exp[-(1/2)px^2], \quad (p \gg 1) \quad (22)$$

in the excess free energy (second term) allows us to calculate the double orientational averages analytically

$$\begin{aligned} \langle \langle |\cos(\varphi' - \varphi)|^p \rangle \rangle &\sim \left(\frac{\beta}{\beta + 2p} \right)^{1/2}, & \text{(N)} \\ &\sim \left(\frac{2}{\pi p} \right)^{1/2}. & \text{(I)} \end{aligned} \quad (23)$$

The value of β is fixed (at a given density) by minimizing the total nematic free energy with respect to the variational parameter. Some rearranging then leads to the following minimization condition

$$\left(\frac{\beta}{p} + 2 \right)^3 - c^2 \frac{\beta}{p} = 0, \quad (24)$$

which has to be solved numerically along with the coexistence equations for the chemical potential and pressure at a given p . These follow straightforwardly from the free energy Eq. (17). The resulting binodals and coexistence chemical potential are shown in Fig. 4 and Fig. 5, respectively.

Another feature we want to point out is that the bifurcation density c^* at large p scales as $c^* \propto p^{1/2}$. The scaling relation can be easily established by making an asymptotic expansion of k_2 from Eq. (15). For the regime $p \gg 1$ one can show with the aid of Eq. (22) that

$$\begin{aligned} k_2(p) &\propto \int_0^\infty d(\varphi' - \varphi) \exp[-(1/2)p(\varphi' - \varphi)^2], \\ &\propto p^{-1/2}, \end{aligned} \quad (25)$$

up to leading order, hence $c^* \propto p^{1/2}$. This result is analogous to the scaling of the critical coupling constant in the LL-simulations of Ref. 18.

B. Isotropic-nematic interface

To assess the properties of the interface between the coexisting isotropic and nematic phases we have to go back to our initial DFT formulation in Section III. If we assume the interface to be flat with a surface normal \hat{x} , the one-particle density will be non-uniform along this direction and depend on the spatial coordinate $x = \mathbf{r} \cdot \hat{x}$

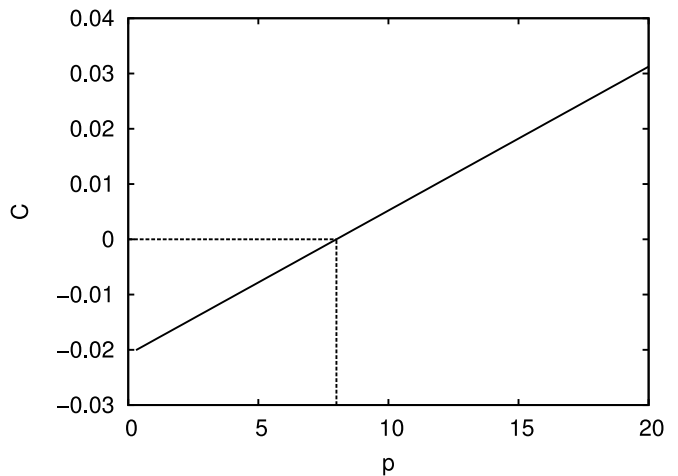


FIG. 1: Landau coefficient C [Eq. (19)] versus p . For $p > 8$ the isotropic-nematic transition is first-order; for smaller p , it is continuous.

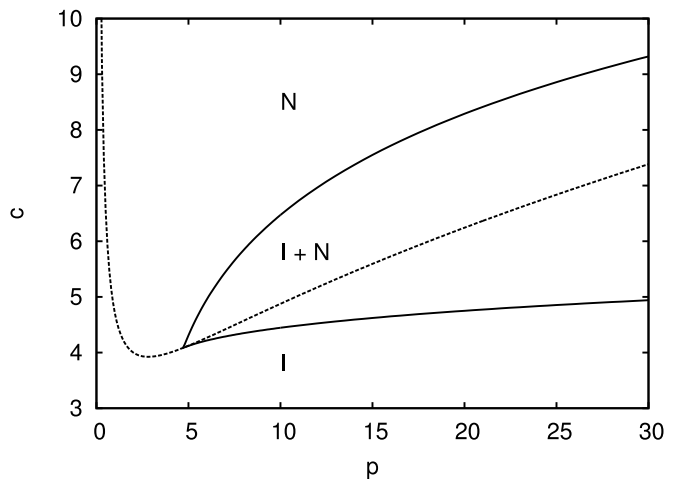


FIG. 2: Theoretical phase diagram. The dashed curve represents the nematic branching line c^* , calculated from Eq. (16). The binodals are given by the solid curves. A tri-critical point is located at $p = 4.7$.

and angle φ . It is a solution of the integral equation Eq. (7) with $\mu = \mu^*$,

$$\begin{aligned} \ln[\mathcal{V}\rho(x, \varphi)] + & \\ \int dx' d\varphi' E_x(\Delta x; \varphi, \varphi'; \vartheta)\rho(x', \varphi') &= \mu^*, \end{aligned} \quad (26)$$

μ^* being the chemical potential at coexistence, and $\Delta x = x' - x$, subject to the boundary conditions

$$\begin{aligned} \rho(x, \varphi) &= \rho_I f_I, & (x \rightarrow -\infty), \\ \rho(x, \varphi) &= \rho_N f_N(\varphi), & (x \rightarrow \infty), \end{aligned} \quad (27)$$

(recall that $\varphi = \arccos(\hat{n} \cdot \hat{w})$). In Eq. (26), the kernel E_x is defined as the pair potential (at fixed orientations)

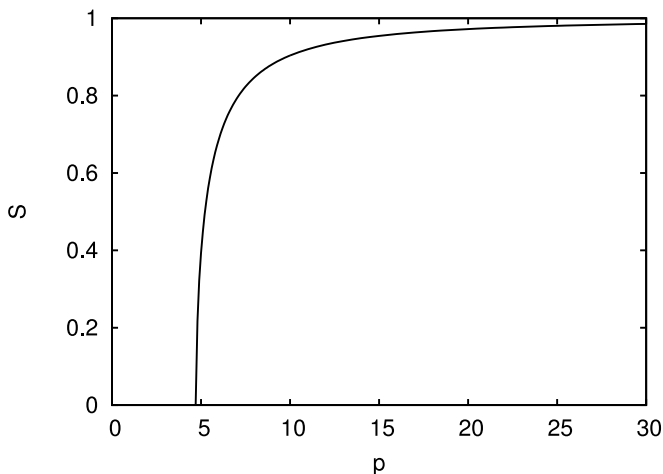


FIG. 3: Nematic order parameter $S = \langle \cos 2\varphi \rangle$ corresponding to the nematic binodal in Fig. 2.

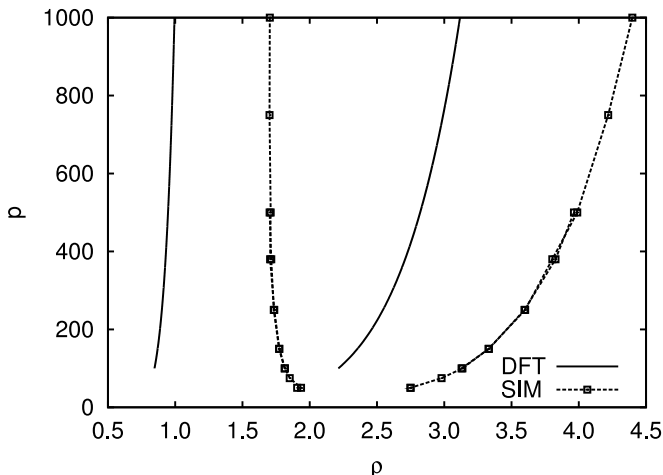


FIG. 4: Phase diagram of the two-dimensional liquid crystal model of Eq. (3) using $\epsilon = 2.5$. The solid curves show the theoretical binodals, obtained using the large p approximation. Plotted is the dimensionless density $\rho = Na^2/A$ of the isotropic phase (left curve) and the nematic phase (right) versus p . Also shown are the corresponding simulation results (squares), where the dashed lines serve to guide the eye.

averaged over the distance Δy perpendicular to \hat{x} along which the system is homogeneous

$$E_x(\Delta x; \varphi, \varphi'; \vartheta) = \int_{-\infty}^{\infty} d\Delta y v(\Delta \mathbf{r}; \varphi, \varphi'; \vartheta). \quad (28)$$

Note that because of the broken spatial symmetry the integral depends implicitly on the *anchoring angle* $\vartheta = \arccos(\hat{n} \cdot \hat{x})$ between the nematic director \hat{n} and the surface normal. This becomes manifest when we focus on the translation-rotation coupling contribution σ in Eq. (4). In explicit form it reads

$$\sigma = 1 + \nu [(\Delta \hat{\mathbf{r}} \cdot \mathcal{R}_\vartheta \hat{\omega})^2 + (\Delta \hat{\mathbf{r}} \cdot \mathcal{R}_\vartheta \hat{\omega}')^2], \quad (29)$$

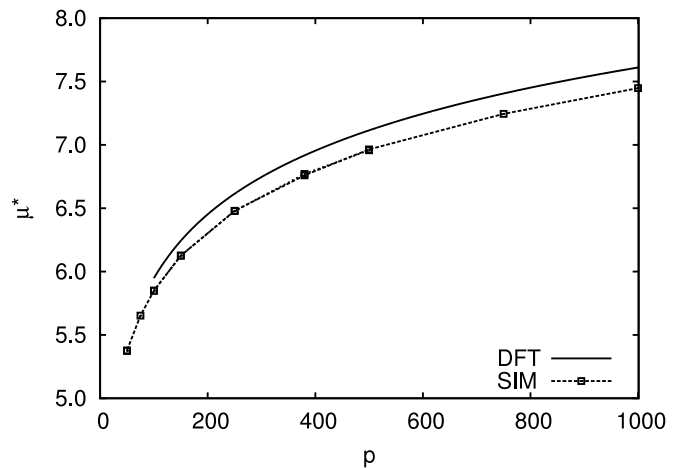


FIG. 5: Coexistence chemical potential μ^* versus p corresponding to Fig. 4. The solid curve is the theoretical result; squares are simulation results.

with $\Delta \hat{\mathbf{r}} = \{\Delta x, \Delta y\}/(\Delta x^2 + \Delta y^2)^{1/2}$ the center-of-mass difference unit vector, $\hat{\omega} = \{\cos \varphi, \sin \varphi\}$ and \mathcal{R}_ϑ the rotation matrix

$$\mathcal{R}_\vartheta = \begin{pmatrix} \cos \vartheta & -\sin \vartheta \\ \sin \vartheta & \cos \vartheta \end{pmatrix}. \quad (30)$$

Clearly, if $\nu = 0$ there is no dependence on ϑ and the interfacial profiles are *identical* for all anchoring angles [30]. If $\nu \neq 0$ the translational and rotational degrees of freedom are coupled and the interfacial properties will in general be dependent upon the anchoring angle. In particular we are interested in the line tension γ which can be extracted from the equilibrium interfacial density profile. Inserting the one-body density into the functional Eq. (7) yields the minimum grand potential

$$\Omega_{\min} = \int d\mathbf{r} \int d\varphi \rho(\mathbf{r}, \varphi) \left\{ \frac{1}{2} \ln[\mathcal{V}\rho(\mathbf{r}, \varphi)] - 1 - \frac{1}{2} \mu^* \right\}. \quad (31)$$

The line tension $\gamma[\mu^*(p), \nu, \vartheta]$ is then obtained from the standard thermodynamic relation $\gamma = (\Omega_{\min} + PA)/L$, with P the coexistence pressure.

In Fig. 6 we show the line tension for $\nu = 0$. To facilitate comparison with simulations later on we will henceforth fix the coupling parameter to $\epsilon = 2.5$. Note that, owing to Eq. (12), changing this value does not give qualitatively different results but merely constitutes a linear shift in γ and ρ . The increase of γ as a function of p reflects the transition becoming strongly first-order at large p . The corresponding interfacial profiles for the density $\rho(x)$ and the nematic order parameter $S(x)$, defined as

$$\begin{aligned} \rho(x) &= \int d\varphi \rho(x, \varphi), \\ S(x) &= \rho^{-1}(x) \int d\varphi \rho(x, \varphi) \cos 2\varphi, \end{aligned} \quad (32)$$

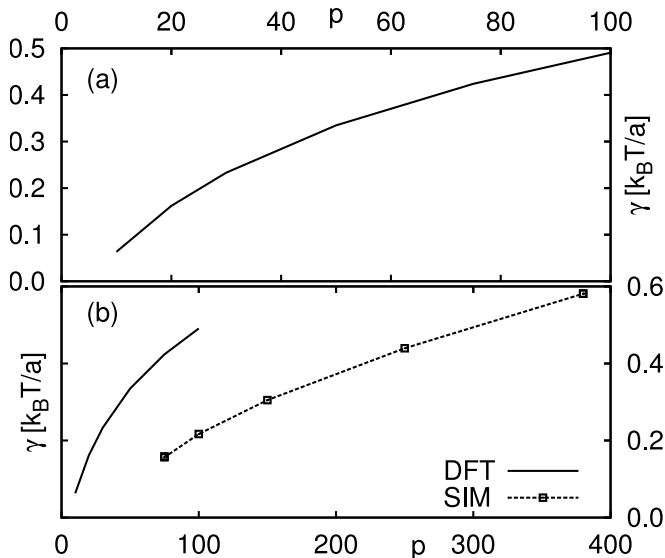


FIG. 6: Line tension γ (in units $k_B T/a$) for $\epsilon = 2.5$ versus p . (a) DFT result. (b) Computer simulation results (squares), together with the DFT result (solid curve) for comparison. Note the different p -range in the above plots.

are shown in Fig. 7. As expected, the interface becomes sharper for large p . For $p = 100$ small density oscillations on the isotropic side occur, which point to a layering effect induced by the interface.

Let us now focus on the anchoring behavior for a fixed value of $p = 75$ and $\nu \neq 0$. The results, summarized in Fig. 8, show a strong dependency of the line tension on the anchoring angle ϑ , especially for $\nu < 0$. Recall that end-to-end pair configurations are energetically more favorable than side-to-side ones in this case. While for $\nu < 0$ the minimal tension is at $\vartheta = 0$ implying *perpendicular* surface anchoring, a positive ν seems to be associated with *parallel* anchoring. Investigations for other p reveal that this phenomenon is robust. Microscopic information extracted from the profiles for $\nu = -0.45$ is shown in Fig. 9. These reveal that the layering effect is considerably influenced by the anchoring angle. In particular, particles show enhanced localization across the interface if the nematic director is forced to be parallel to the interface.

An even more dramatic effect is encountered if we lower $\nu \rightarrow -0.5$, see Fig. 10. Note that, for $\nu = -0.5$, the end-to-end configurations have zero repulsion and are therefore strongly favored. This explains the tendency of the system to form string like clusters along the interface as indicated by the sharp density peaks in Fig. 10. However $\nu = -0.5$ seems to be a rather pathological case. The density modulations penetrate deeply into the isotropic bulk which raises strong suspicions as to whether the isotropic fluid state is stable against clustering or crystallization. It remains to be checked by simulations whether the IN transition is really pre-empted by a freezing transition in this case.

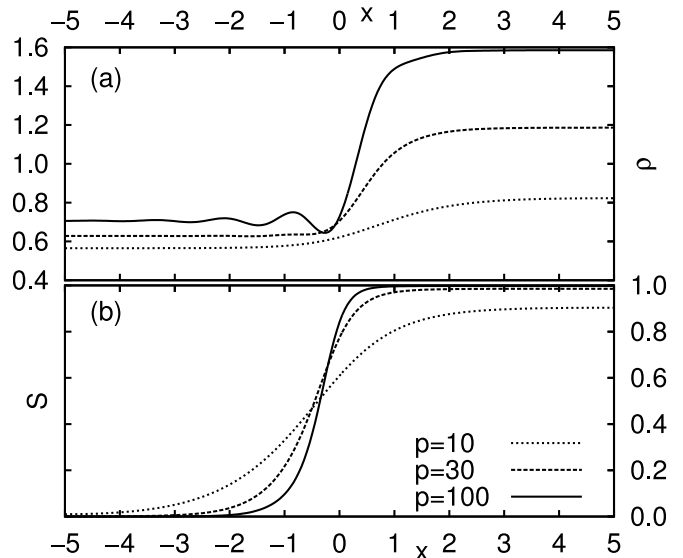


FIG. 7: Interfacial profiles for (a) the density $\rho(x)$ and (b) the nematic order parameter $S(x)$ for $\nu = 0$.

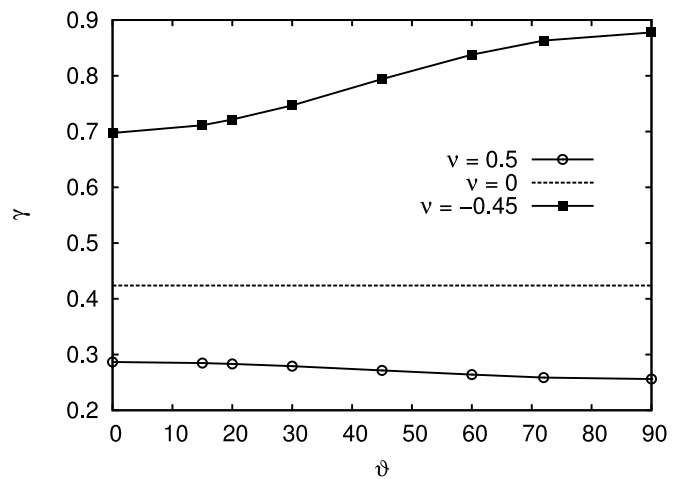


FIG. 8: Line tension γ (in units $k_B T/a$) versus anchoring angle ϑ (in degrees), for several values of ν as indicated.

IV. COMPUTER SIMULATION

Next, we will confirm some of the theoretical results using computer simulation. To this end, grand canonical (GC) Monte Carlo simulations [31, 32] are performed, at chemical potential μ , for the model of Eq. (3) using $\epsilon = 2.5$. Again, for the radial part, we take the step function of Eq. (5). In this work, we restrict the simulations to the case $\nu = 0$ in Eq. (3). A computer simulation study of anchoring effects, predicted by the theory to occur when $\nu \neq 0$, will be postponed to a future publication.

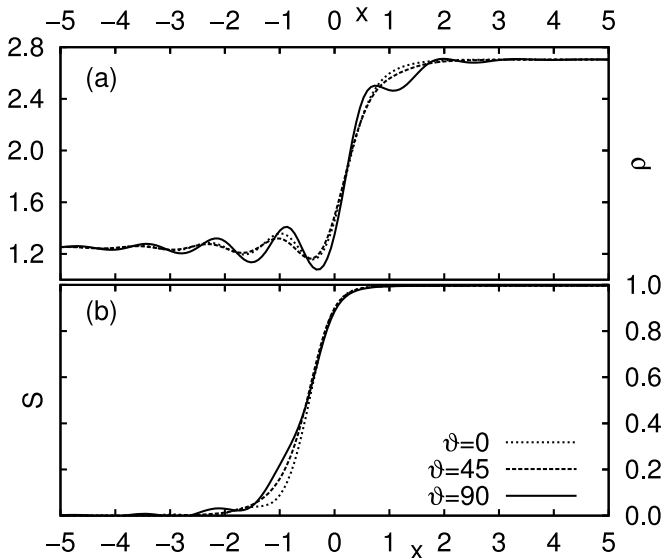


FIG. 9: Interfacial profiles for $p = 75$, $\nu = -0.45$ at different anchoring angles ϑ (in degrees).

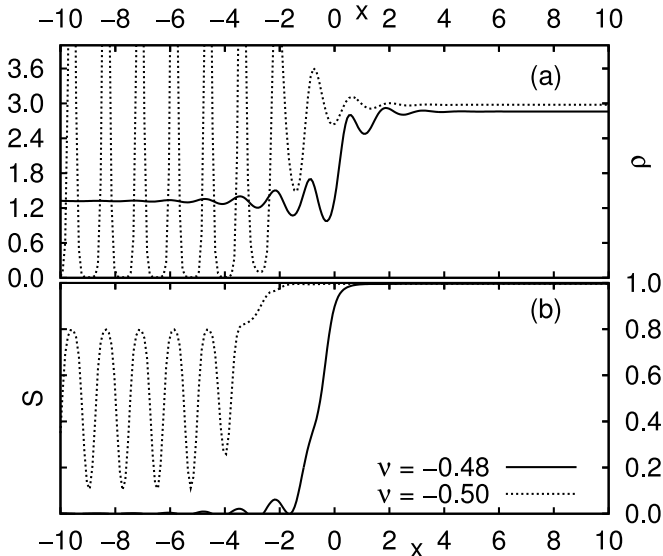


FIG. 10: Interfacial profiles for $p = 75$ and anchoring angle $\vartheta = 90$ degrees.

A. Finite-size scaling results for $p = 75$

We begin the simulations using $p = 75$ in Eq. (3). Inspired by our theoretical results, we expect that, for $p = 75$, a first-order phase transition should occur, when the chemical potential is tuned to its coexistence value μ^* . In GC simulations, μ^* is determined from the distribution $P_L(\rho, \mu)$, defined as the probability to observe a particle density ρ in the system. In order to also simulate the regions of low probability, a biased sampling scheme is implemented [33, 34]. The distribution $P_L(\rho, \mu)$ de-

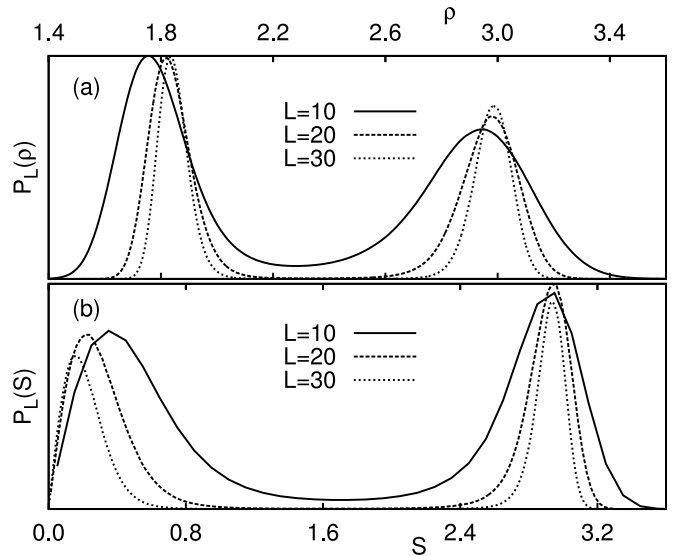


FIG. 11: (a) Coexistence distributions $P_L(\rho, \mu)$ for various system sizes L as indicated, with $\rho = Na^2/A$ the dimensionless particle density. The coexistence between the two phases is manifested by “equal-area” under the peaks. (b) The corresponding distributions $P_L(S)$ of the nematic order parameter S , given by Eq. (34).

pends on the chemical potential μ , as well as on the size of the $L \times L$ simulation square (periodic boundary conditions are assumed). At $\mu = \mu^*$, $P_L(\rho, \mu)$ becomes bimodal, with two peaks of equal area. In computer simulations, the transition can thus be located by varying μ until the “equal-area” criterion is obeyed.

Indeed, we find that bimodal density distributions can be realized in this way. Fig. 11(a) gives some examples for various system sizes L . By increasing L , the peaks become more narrow. This is to be expected because, in the thermodynamic limit $L \rightarrow \infty$, one has a sharp transition, and, consequently, a distribution featuring two δ -peaks. In addition, closer inspection of Fig. 11(a) also reveals a finite-size effect in the peak positions. Finite-size effects at first-order phase transitions have received considerable attention [35, 36, 37]. We believe that the current state-of-the-art in this field is the rigorous treatment of Borgs and Kotecky [37]. More precisely, for two-phase coexistence data obtained using the “equal-area” rule, an exponential L -dependence is predicted

$$R \equiv |X_L - X_\infty| \leq \mathcal{O}(e^{-\tau L}). \quad (33)$$

Here, X_L is the property of interest as obtained in the finite system of size L , X_∞ the corresponding value in the thermodynamic limit, and τ a constant.

In Fig. 12(a), we show the position ρ_L of the high-density (nematic) peak of $P_L(\rho, \mu)$ as a function of L . Next, we use Eq. (33) to estimate the density ρ_∞ of the nematic phase in the thermodynamic limit. To this end we have plotted, in Fig. 12(b), the logarithm of R as a function of system size L . Here, ρ_∞ was taken to be a

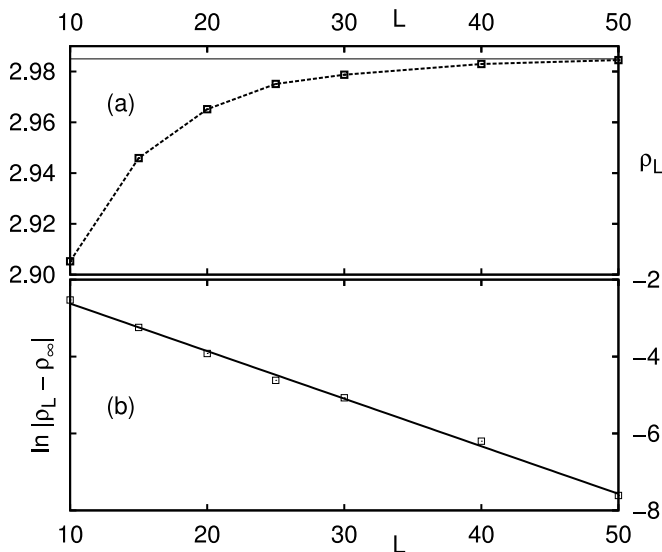


FIG. 12: Finite-size scaling of the position of the high-density peak in $P_L(\rho, \mu)$ of Fig. 11(a). (a) Peak position ρ_L as a function of L . The horizontal line marks the density ρ_∞ in the thermodynamic limit. (b) Finite-size scaling analysis using Eq. (33). The straight line is a linear fit; see details in text.

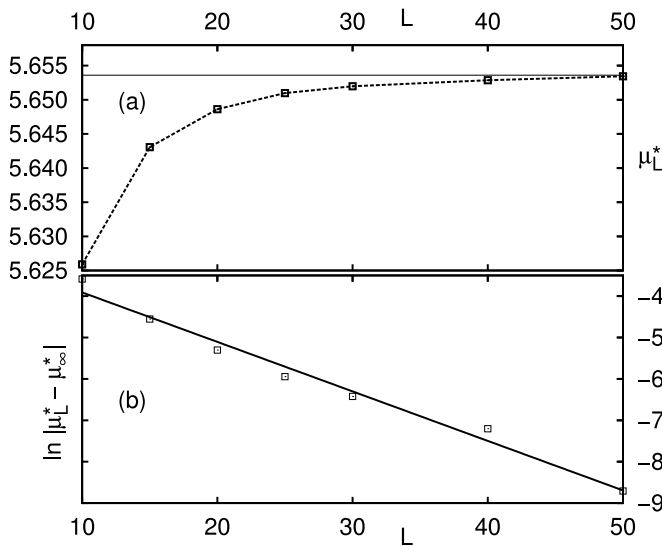


FIG. 13: Finite-size scaling of the coexistence chemical potential. (a) μ_L^* as a function of L . The horizontal line marks the coexistence chemical potential μ_∞^* in the thermodynamic limit. (b) Finite-size scaling analysis using Eq. (33). The straight line is a linear fit; see details in text.

fit parameter, and tuned until the graph of $\ln R$ versus L became linear. For $\rho_\infty \approx 2.985$, we find that $\ln R$ indeed becomes linear in L , which thus serves as our best estimate of the nematic density in the thermodynamic limit. For completeness, this estimate has also been marked in Fig. 12(a) as the horizontal line. The density of the low-density (isotropic) peak can be obtained analogously.

The corresponding scaling plot is qualitatively similar to Fig. 12 and therefore not shown here. For the density of the isotropic phase in the thermodynamic limit, we obtain $\rho_\infty \approx 1.850$.

In addition, we also observe an L -dependence in the coexistence chemical potential μ_L^* . Recall that μ_L^* corresponds to the chemical potential at which “equal-area” in $P_L(\rho, \mu)$ of the *finite* system is observed. Shown in Fig. 13(a) is μ_L^* versus L . Again, Borgs and Kotecky predict an exponential L -dependence given by Eq. (33). We may therefore estimate μ_∞^* as before, by plotting $\ln R$ versus L , using for μ_∞^* that value at which the data become linear. The result is shown in Fig. 13(b). Again, the data follow the straight line quite well, and we conclude $\mu_\infty^* \approx 5.6536$.

It is also of interest to consider the distribution $P_L(S)$ at coexistence, with S the nematic order parameter. Here, we define S as the maximum eigenvalue of the orientational tensor

$$Q_{\alpha\beta} = \frac{1}{A} \sum_{i=1}^N (2d_{i\alpha}d_{i\beta} - \delta_{\alpha\beta}), \quad (34)$$

with $d_{i\alpha}$ the α component ($\alpha = x, y$) of the orientation $\hat{\omega}_i$ of molecule i , $\delta_{\alpha\beta}$ the Kronecker delta, N the number of particles, and system area $A = L^2$. For an isotropic phase, in the thermodynamic limit, S equals zero. For a “true” nematic phase, i.e. with long-range order, one has $S > 0$ in the thermodynamic limit. Note that we have normalized Eq. (34) with the system area A , and not with N as is usually done. The reason to normalize with respect to A is that, in the GC ensemble, N is a fluctuating quantity. Note also that, for a perfectly aligned phase, S becomes identical to the particle density N/A .

Several distributions $P_L(S)$ are shown in Fig. 11(b). We emphasize that all these distributions were obtained using that value of μ at which “equal-area” in $P_L(\rho, \mu)$ was obtained. The data of Fig. 11(b) are quite stunning. On the one hand, we observe a pronounced shift of the lower-peak toward $S \rightarrow 0$. This is to be expected, since this peak corresponds to the isotropic phase. Note that the L -dependence of the isotropic peak does not reveal any physical information: an ideal gas of rods would reveal the same effect. The L -dependence of S in the isotropic phase is purely a numerical artifact. It stems from the fact that S is positive, since always the *maximum* eigenvalue of the orientational tensor is taken. Consequently, the distribution of S in the isotropic phase *cannot* be gaussian around $S = 0$. Instead, the distribution is “skewed”, with the peak *always* being located at $S > 0$. As the system size is increased, the isotropic peak shifts to zero, see the discussion by Eppenga and Frenkel [38], precisely what we observe.

In contrast, on the scale of Fig. 11(b), the nematic peak appears to be rather insensitive to the system size L . In fact, finite-size scaling of the nematic peak position suggests that a finite value S_∞ in the thermodynamic limit is maintained, see Fig. 14. Shown in Fig. 14(a) is

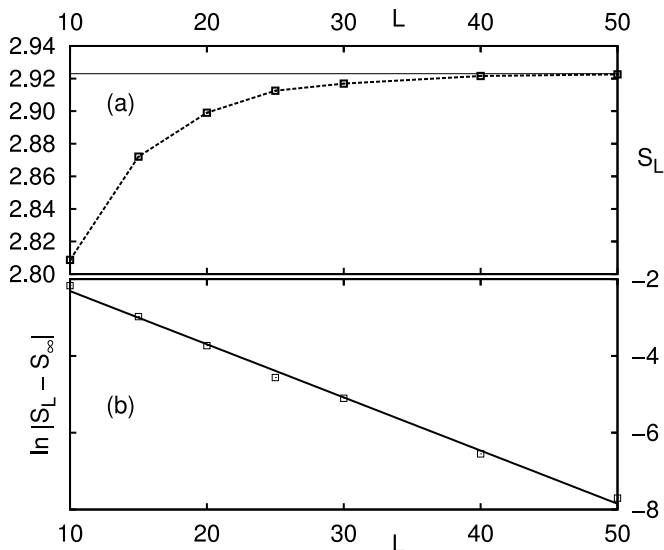


FIG. 14: Finite-size scaling of the position of the nematic peak in $P_L(S)$ of Fig. 11(b). (a) Peak position S_L as a function of L . The horizontal line marks the nematic order parameter S_∞ in the thermodynamic limit. (b) Finite-size scaling analysis using Eq. (33). The straight line is a linear fit; see details in text.

the nematic peak position S_L as a function of L . The data are quite interesting, because they show an *increase* of nematic order with increasing system size L . Shown in Fig. 14(b) is the result of the finite-size scaling analysis using Eq. (33). Again, S_∞ was obtained by tuning, until the best collapse of the data onto a straight line occurred. For the nematic order parameter in the thermodynamic limit, we obtain $S_\infty \approx 2.923$. Note that, for $\nu = 0$, the liquid crystal potential of Eq. (3) is separable. For this special case, Straley has proved the *absence* of long-range nematic order in the thermodynamic limit [19]. In other words, S_∞ should become zero, while our finite-size analysis, in contrast, suggests that S_∞ remains finite. For the XY-model in two dimensions, it has been shown that the decay of magnetic order with system size is so slow, one would need a sample “the size of Texas” [39] to see it. The most likely explanation is therefore that something similar also takes place in our liquid crystal model, and that the data of Fig. 14(a) will eventually “turn-over” and decay to zero.

Next, we consider the logarithm of the distributions, which essentially reflect *minus* the free energy of the system. Shown in Fig. 15 is $\ln P_L(S)$ for several system sizes L . Again, we emphasize that the distributions were obtained using that value of μ at which “equal-area” in $P_L(\rho, \mu)$ was obtained. For each distribution $\ln P_L(S)$, we may read-off the average peak height ΔF , measured with respect to the minimum between the peaks. By increasing the size of the system, ΔF increases as well. As was shown by Binder, ΔF corresponds to the free-energy cost of having two interfaces in the system [40].

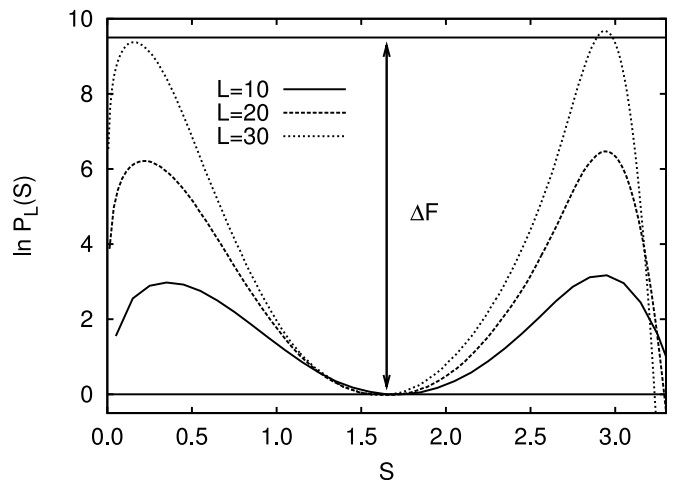


FIG. 15: Distributions $\ln P_L(S)$ for various system sizes L as indicated. Also marked is ΔF for the $L = 30$ system.

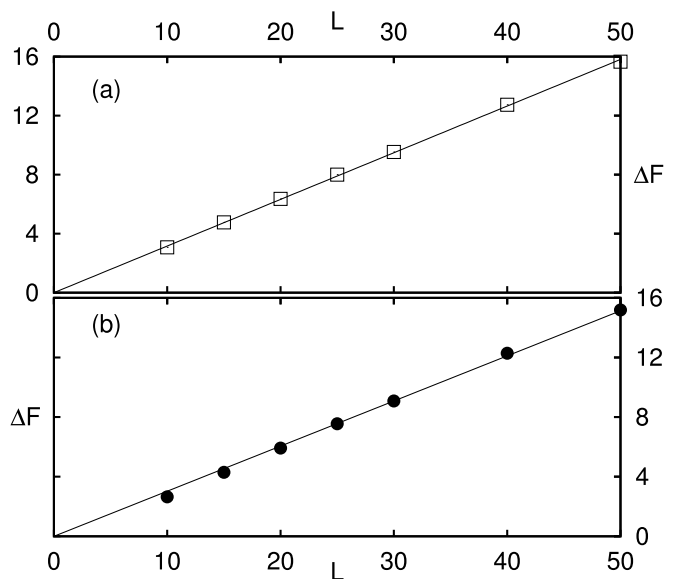


FIG. 16: (a) Free energy barrier ΔF , extracted from the distributions $\ln P_L(S)$ of Fig. 15, as a function of L . The straight line is a fit to Eq. (35). (b) Same as (a), but with ΔF extracted from $\ln P_L(\rho, \mu)$.

More precisely, in two dimensions, we expect that

$$\Delta F = 2\gamma L, \quad (35)$$

with γ the line tension (the factor of two stems from the use of periodic boundary conditions, which lead to the formation of two interfaces in the system, see also the snapshot of Fig. 17). Shown in Fig. 16(a) is ΔF as a function of L ; the data are indeed well described by a straight line through the origin. From the slope of the line, we obtain $\gamma = 0.158 k_B T/a$. Of course, we may also read-off the barrier in $\ln P_L(\rho, \mu)$, shown in Fig. 16(b). Again, a linear increase of ΔF is observed, and from the

slope of the line we obtain $\gamma = 0.151 k_B T/a$, which is very close to our previous estimate.

In summary, and in agreement with our theoretical results, we find that an exponent $p = 75$ is high enough to induce a first-order transition in the *off-lattice* liquid crystal model of Eq. (3). The scaling of the coexisting densities with system size are well described by what is expected for such a transition. The same also holds for the growth of the free energy barrier ΔF . An interesting and unexpected result, which certainly requires further elaboration, is the scaling of the nematic order parameter, see Fig. 14. If the trend continues for $L \rightarrow \infty$, long-range nematic order in a two-dimensional liquid crystal would, after all, be possible.

B. Results for different p

We have also measured the coexistence densities, chemical potential, and line tension for different values of p , while keeping $\nu = 0$ and $\epsilon = 2.5$. Here, we did not perform a detailed finite-size scaling analysis. Instead, the data for $p \neq 75$ were obtained in a single simulation of a (reasonably large) system. In Fig. 4, we show the density of the isotropic phase, and of the nematic phase, as a function of p . Note that the region in between the curves corresponds to phase coexistence. If one performs a simulation in this region, for example by keeping the density fixed, snapshots strikingly reveal the two-phase coexistence, see Fig. 17. Shown in Fig. 5 is the coexistence chemical potential μ^* versus p , compared to the DFT result. Finally, in Fig. 6(b), we show the line tension versus p .

V. DISCUSSION AND SUMMARY

In summary, we have provided strong evidence that *off-lattice* liquid crystals in two dimensions can also undergo first-order phase transitions. To this end, the pair potential of Eq. (3) was introduced, constructed to be purely repulsive, short-ranged, and to obey inversion symmetry. The first-order transition takes place when the pair potential becomes sufficiently “sharp and narrow”, i.e. for a sufficiently large exponent p in Eq. (3). A simple DFT calculation puts the threshold value at around $p = 8$. When $p > 8$, the theory predicts a first-order transition from a low-density (isotropic) phase, to a high-density (nematic) phase. In other words, there is a finite density gap between the two phases, as well as a jump in the nematic order parameter.

An important conclusion of this work is that many of the trends predicted by the theory, also appear in the computer simulations. In other words, key properties of Eq. (3) are already captured at the mean-field level. This finding is somewhat surprising because, in low spatial dimension, mean-field is typically assumed to be unreliable. The simulations, in agreement with the theory,

find strong γ evidence of a first-order transition, already at $p > 50$. Note that we have backed our simulations with a detailed investigation of finite-size effects, and that these were shown to be consistent with a first-order phase transition. We have not determined in our simulations the precise value of p where the crossover from continuous to first-order occurs, since such simulations would be extremely time consuming, but we expect this will exceed the theoretical bound $p = 8$ significantly.

Nevertheless, for those values of p where the simulations do observe the first-order transition, a profound density gap between the two coexisting phases is found, see the phase diagram of Fig. 4. In the limit of large p , theory and simulation are in qualitative agreement: both show an increase in density of the nematic phase with p , while the density of the isotropic phase is much less sensitive to p . At lower p , qualitative discrepancies arise, but these can be attributed to the large- p approximation used by the theory, which obviously breaks down here. Interestingly, when comparing the coexistence chemical potential μ^* between theory and simulation, see Fig. 5, the agreement is remarkably good, also at low p . Apparently, the breaking-down of the large- p approximation does not affect μ^* as much as it does the coexistence densities. With regards to the line tension, see Fig. 6, the agreement between theory and simulation is merely qualitative: by increasing p , the tension increases in both cases, but the actual numerical values differ profoundly. A possible explanation may be the presence of capillary-wave interface fluctuations. These fluctuations are neglected in the theory, while the simulation snapshot of Fig. 17 suggests that interface fluctuations are actually quite strong.

A rather controversial result of this work is the value of the nematic order parameter S in the nematic phase. The DFT result, see Fig. 3, predicts rather large values of S , once the transition has become first-order. Of course, in realistic systems, one always has defects, which are expected to destroy nematic order in the thermodynamic limit. Since such defects are discarded by the theory, we expect that Fig. 3 is merely an artifact, and that realistic systems in the thermodynamic limit will always have $S = 0$, regardless the value of p . Still, it is somewhat surprising that our computer simulations also suggest that $S > 0$, see Fig. 14, and that the finite-size effects in our data are *not* compatible with a decay of S to zero. At this point, the most likely explanation is that the decay of S with system size only shows-up in macroscopically large samples, which are clearly out of reach in any foreseeable simulation.

Note that our theory has also made a number of intriguing predictions for the case where the translational and orientational degrees of freedom are coupled, i.e. when $\nu \neq 0$. In this case, strong anchoring effects are predicted, as well as the possibility of the isotropic-to-nematic transition being pre-empted by freezing. Since our particles are ultrasoft, the formation of stable aggregate or cluster mesophases as encountered in various

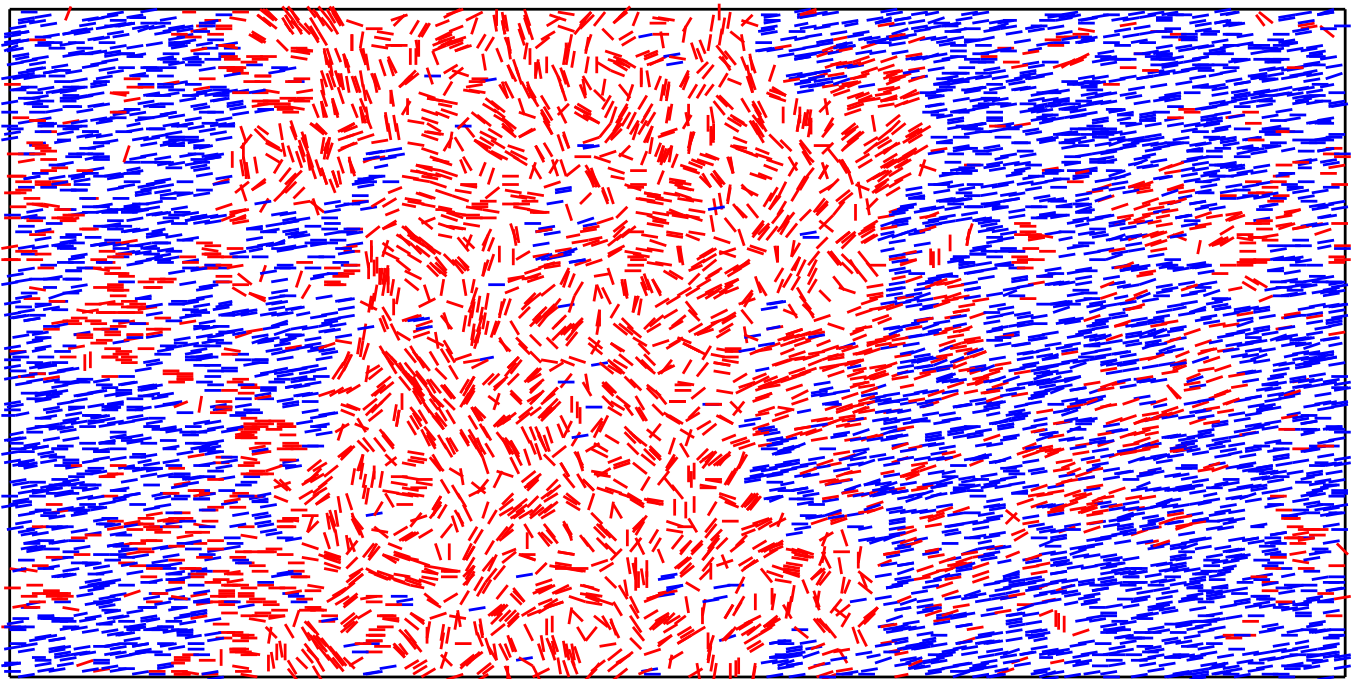


FIG. 17: Simulation snapshot obtained in the coexistence region for $p = 60$. Each line segment represents a particle. Clearly visible is that the system has phase-separated into an isotropic domain, and a nematic domain (where we leave open the question whether the nematic phase exhibits true long-range order, or only quasi long-range order). Note also that the interfaces are not flat, and that they appear to be decorated with capillary waves.

soft-sphere systems [41, 42] is also possible. All these scenarios need to be verified by computer simulation. We are currently developing new simulation methodology to study anchoring effects at the isotropic-nematic interface; some preliminary information about the method is already available [43]. The application of these new techniques to the 2D liquid crystal model of the present work is therefore postponed to a future publication.

Of course, it would be interesting if some of our findings could be confirmed in experiments. As we had already remarked in the Introduction, the condition of phase coexistence is obtained straightforwardly by keeping the density fixed at some value in the coexistence region. The problem will most likely be to achieve sufficiently “sharp and narrow” interactions. One possibility that we envision is to use a mixture of colloidal rods and non-adsorbing polymers. Despite the fact that colloidal rods cannot overlap, unlike the particles considered here, and that the addition of polymer renders the *effective* rod interactions *attractive*, which may induce an additional gas-liquid phase separation, we believe a first-order isotropic-nematic phase transition could be feasible. In particular, looking at the phase diagrams reported for 3D rod-polymer mixtures [44] we anticipate that the strong polymer-induced widening of the isotropic-nematic coexistence region carries over to 2D systems as well, and might induce a first-order transition. A prerequisite for this scenario is that both the size ratio (of rod length to

polymer radius of gyration) and the polymer concentration are sufficiently large.

Finally, we would like to remind the reader that the original idea of this work, namely to use “sharp and narrow” interactions is not new, and goes back to the work of Ref. 12. Here, the approximate correspondence between generalized XY-models and the Potts model [45] was already exploited to demonstrate the possibility of having a first-order transition in a 2D spin system with continuous degrees of freedom. The extension of this work has been to apply the same ideas to *off-lattice* liquid crystals. Nevertheless, the approximate link to the Potts model can still be uncovered, using $q \propto p^{1/2}$ [13]. Here, p is the exponent in Eq. (3), and q the number of Potts states. Note that this relation is valid only asymptotically for large p . Many of the results of this work, for example the cross-over from a continuous to a first-order transition (Fig. 1), the variation of μ^* with p (Fig. 5), and even the increase of the line tension with p (Fig. 6), have their analogues in the 2D Potts model (see for example Ref. 46, where an explicit formula for the line tension of the Potts model is given).

Acknowledgments

This work was supported by the *Deutsche Forschungsgemeinschaft* under the SFB-TR6 (project section D3).

-
- [1] J. M. Kosterlitz, *J. Phys. C* **7**, 1046 (1974).
- [2] P. A. Lebowitz and G. Lasher, *Phys. Rev. A* **6**, 426 (1972).
- [3] N. D. Mermin and H. Wagner, *Phys. Rev. Lett.* **17**, 1133 (1966).
- [4] D. Frenkel and R. Eppenga, *Phys. Rev. A* **31**, 1776 (1985).
- [5] M. A. Bates and D. Frenkel, *J. Chem. Phys.* **112**, 10034 (2000).
- [6] M. C. Lagomarsino, M. Dogterom, and M. Dijkstra, *J. Chem. Phys.* **119**, 3535 (2003).
- [7] J. Tobochnik and G. V. Chester, *Phys. Rev. A* **27**, 1221 (1983).
- [8] J. M. Kosterlitz and D. J. Thouless, *J. Phys. C* **5**, L124 (1972).
- [9] J. M. Kosterlitz and D. J. Thouless, *J. Phys. C* **6**, 1181 (1973).
- [10] A. I. Farinas-Sanchez, R. Paredes, and B. Berche, *Phys. Rev. E* **72**, 031711 (2005).
- [11] B. Berche and R. Paredes, *Cond. Matt. Phys.* **8**, 723 (2005).
- [12] E. Domany, M. Schick, and R. H. Swendsen, *Phys. Rev. Lett.* **52**, 1535 (1984).
- [13] H. W. J. Blöte, W. Guo, and H. J. Hilhorst, *Phys. Rev. Lett.* **88**, 047203 (2002).
- [14] A. Jonsson, P. Minnhagen, and M. Nylén, *Phys. Rev. Lett.* **70**, 1327 (1993).
- [15] A. C. D. van Enter, S. Romano, and V. A. Zagrebnov, *J. Phys. A* **39**, L439 (2006).
- [16] A. C. D. van Enter and S. B. Shlosman, *Commun. Math. Phys.* **255**, 21 (2005).
- [17] A. C. D. van Enter and S. B. Shlosman, *Phys. Rev. Lett.* **89**, 285702 (2002).
- [18] R. L. C. Vink, *Phys. Rev. Lett.* **98**, 217801 (2007).
- [19] J. P. Straley, *Phys. Rev. A* **4**, 675 (1971).
- [20] R. Evans, *Adv. Phys.* **28**, 143 (1979).
- [21] N. Grewe and W. Klein, *J. Math. Phys.* **64**, 1729 (1977).
- [22] A. Lang, C. N. Likos, M. Watzlawek, and H. Löwen, *J. Phys.: Condens. Matter* **12**, 5087 (2000).
- [23] A. J. Archer, *J. Phys.: Condens. Matter* **17**, 1405 (2005).
- [24] M. Rex, H. H. Wensink, and H. Löwen, *Phys. Rev. E* **76**, 023708 (2007).
- [25] R. F. Kayser and H. J. Raveché, *Phys. Rev. A* **17**, 2067 (1978).
- [26] B. M. Mulder, *Phys. Rev. A* **39**, 360 (1989).
- [27] This can be shown by replacing $|\cos(\varphi' - \varphi)|$ in Eq. (15) by the Onsager kernel $-\sin(\varphi' - \varphi)$, see Ref. 19. Both kernels yield the same coefficient $c_2 = 4/(3\pi)$, and hence the same bifurcation density $c^* = 3\pi/2$.
- [28] J. Herzfeld, A. E. Berger, and J. W. Wingate, *Macromolecules* **17**, 1718 (1984).
- [29] T. Odijk and H. N. W. Lekkerkerker, *J. Phys. Chem.* **89**, 2090 (1985).
- [30] The ϑ -dependence also vanishes for the bulk case, as it should. This can easily be verified by carrying out the total spatial integral of σ [cf. Eq. (9)].
- [31] D. Frenkel and B. Smit, *Understanding Molecular Simulation* (Academic Press, San Diego, 2001).
- [32] D. P. Landau and K. Binder, *A Guide to Monte Carlo Simulations in Statistical Physics* (Cambridge University Press, Cambridge, 2000).
- [33] P. Virnau and M. Müller, *J. Chem. Phys.* **120**, 10925 (2004).
- [34] R. L. C. Vink, S. Wolfsheimer, and T. Schilling, *J. Chem. Phys.* **123**, 074901 (2005).
- [35] K. Vollmayr, J. D. Reger, M. Scheucher, and K. Binder, *Z. Phys. B* **91**, 113 (1993).
- [36] K. Binder and D. P. Landau, *Phys. Rev. B* **30**, 1477 (1984).
- [37] C. Borgs and R. Kotecky, *J. Stat. Phys.* **61**, 79 (1990).
- [38] R. Eppenga and D. Frenkel, *Mol. Phys.* **52**, 1303 (1984).
- [39] S. T. Bramwell and P. C. W. Holdsworth, *Phys. Rev. B* **49**, 8811 (1994).
- [40] K. Binder, *Phys. Rev. A* **25**, 1699 (1982).
- [41] B. M. Mladek, D. Gottwald, G. Kahl, M. Neumann, and C. N. Likos, *Phys. Rev. Lett.* **96**, 045701 (2006).
- [42] M. A. Glaser, G. M. Gason, R. D. Kamien, A. Košmrlj, C. D. Santangelo, and P. Ziherl, *Europhys. Lett.* **78**, 46004 (2007).
- [43] R. L. C. Vink, preprint <http://arxiv.org/abs/0706.2424> (2007).
- [44] H. N. W. Lekkerkerker and A. Stroobants, *Nuovo Cimento D* **16**, 949 (1994).
- [45] F. Y. Wu, *Rev. Mod. Phys.* **54**, 235 (1982).
- [46] C. Borgs and W. Janke, *J. Phys. I France* **2**, 2011 (1992).